Inorg. Chem. **2009**, *48*, 3027−3038

Heterotetranuclear Oxalato-Bridged $Re^{IV}_3M^{II}$ (M = Mn, Fe, Co, Ni, Cu) Complexes: A New Example of a Single-Molecule Magnet (M = Ni)

José Martínez-Lillo,[†,‡] Donatella Armentano,[‡] Giovanni De Munno,[*,‡] Wolfgang Wernsdorfer,[⊥] Juan Modesto Clemente-Juan,[†,§] J. Krzystek,[¶] Francesc Lloret,[†] Miguel Julve,[†] and Juan Faus[*,†]

Departament de Química Inorgànica/Instituto de Ciencia Molecular, Facultat de Química, Universitat de València, Avenida Dr. Moliner 50, 46100 Burjassot, València, Spain, Dipartimento di Chimica, Università della Calabria, via P. Bucci 14/c, 87030 Arcavacata di Rende, Cosenza, Italy, Institut Néel-CNRS, BP 166, 25 Avenue des Martyrs, 38042 Grenoble Cedex 9, France, and National High Magnetic Field Laboratory (NHMFL), Florida State University, Tallahassee, Florida 32310

Received November 10, 2008

The use of the mononuclear species $(NBu_4)_2[Re^{IV}Cl_4(ox)]$ (NBu_4^+ = tetra-*n*-butylammonium cation; ox = oxalate dianion) as a ligand toward fully solvated divalent first-row transition-metal ions affords the tetranuclear complexes $(NBu_4)_4[\{Re^{IV}Cl_4(\mu\text{-ox})\}_3M^{II}]$ with M = Mn (**1**), Fe (**2**), Co (**3**), Ni (**4**), and Cu (**5**). Their structure is made up of discrete $[\{ReCl_4(\mu\text{-ox})\}_3M]^{4-}$ anions and bulky NBu_4^+ cations. The complexes **2**−**5** crystallize in the triclinic system with space group $P\bar{1}$; **2** and **5** as well as **3** and **4** are isostructural. The Re and M atoms exhibit somewhat distorted $ReCl_4O_2$ and MO_6 octahedral surroundings, with the oxalate groups adopting the bis-bidentate bridging mode. Magnetic susceptibility measurements on polycrystalline samples of **1**−**5** in the temperature range 1.9−300 K show the occurrence of intramolecular antiferromagnetic [$J = -1.30$ cm^{-1} (**1**)] and ferromagnetic couplings [$J = +1.62$ (**2**), $+3.0$ (**3**), $+16.3$ (**4**), and $+4.64$ cm^{-1} (**5**)], with the Hamiltonian being defined as $H = -J[S_M(S_{Re1} + S_{Re2} + S_{Re3})]$. Compound **4** is the first example of an oxalato-bridged heterometallic species that behaves as a single-molecule magnet with a ground-state spin $S = {}^{11}/_2$ and $D = -0.8(1)$ cm^{-1}, as shown by the study of its static and dynamic magnetic properties and a high-frequency electron paramagnetic resonance study on polycrystalline samples together with detailed micro-SQUID measurements on single crystals.

Introduction

Since their discovery,[1] single-molecule magnets (SMMs) have been the subject of deep studies and continuous development.[2] These magnetic systems are of particular interest in physics, chemistry, and materials science because of their fundamental properties (for instance, quantum phenomena and finite-size effects) as well as their possible applications in magnetic devices (molecular units for data storage or quantum computing in the near future).[3] The main requirements to have a double minimum potential for the reversal of the magnetic moment in the so-called SMMs are a ground state with both high spin (S) and large negative axial anisotropy [measured by the axial zero-field-splitting (zfs) parameter (D)], combined with negligible intermolecular interactions. The relaxation barrier is given by $U = S^2|D|$ if S is an integer or $U = (S^2 - {}^1/_4)|D|$ if S is a half-integer.

Most of the reported examples of SMMs deal with homometallic Mn polynuclear complexes where the source of magnetic anisotropy is due to the presence of Mn^{III} metal ions that exhibit an axial Jahn−Teller distortion. The need

* To whom correspondence should be addressed. E-mail: demunno@unical.it (G.D.), juan.faus@uv.es (J.F.).
† Universitat de València.
‡ Università della Calabria.
§ Fundación General de la Universitat de València.
⊥ Institut Néel-CNRS.
¶ Florida State University.

(1) (a) Sessoli, R.; Gatteschi, D.; Novak, M. A. *Nature* **1993**, *365*, 141. (b) Sessoli, R.; Tsai, H.; Schake, A. R.; Wang, S.; Vicent, J. B.; Folting, K.; Gatteschi, D.; Christou, G.; Hendrickson, D. N. *J. Am. Chem. Soc.* **1993**, *115*, 1804.
(2) (a) Ritter, S. K. *Chem. Eng. News* **2004**, *82*, 29. (b) Christou, G. *Polyhedron* **2005**, *24*, 2065.
(3) (a) Wernsdorfer, W.; Sessoli, R. *Science* **1999**, *284*, 133. (b) Leuenberger, M. N.; Loss, D. *Nature* **2001**, *410*, 789. (c) Wernsdorfer, W.; Aliaga-Alcaide, N.; Hendrickson, D. N.; Christou, G. *Nature* **2002**, *416*, 406. (d) Gatteschi, D.; Sessoli, R. *Angew. Chem., Int. Ed.* **2003**, *42*, 268. (e) Barbara, B. *Inorg. Chim. Acta* **2008**, *361*, 3371. (f) Bogani, L.; Wernsdorfer, W. *Nat. Mater.* **2008**, *7*, 179.

10.1021/ic8021497 CCC: $40.75
Published on Web 03/10/2009

for a larger energy barrier to get high-temperature SMMs, on the one hand, and a better understanding of the quantum tunneling of the magnetization (which being governed by transverse anisotropy can be observed at lower temperatures), on the other hand, oriented this research activity toward the heterometallic 3d−4f systems, as illustrated by very recent reports.[4] SMMs containing only a single lanthanide metal ion as the magnetic center have also been reported.[5] Another alternative strategy can be to study systems involving 4d or 5d metal ions, which have been much less explored. *A priori* the large values for anisotropy and spin−orbit coupling as well as the greater orbital diffuseness that they exhibit make them very appealing and interesting. In fact, only a few examples of such compounds have been studied and well-characterized, with all of them being cyanide-containing species: (i) the complex $K[\{Mo^{V}(Me_3tacn)(CN)_3\}_6Mn^{II}](ClO_4)_3$ (Me_3tacn = *N*,*N*′,*N*″-trimethyl-4,7-triazacyclononane), which was found to be the first example of a cyanide-bridged compound behaving as a SMM;[6] (ii) a family of cubic polynuclear compounds of Re^{II} and several 3d metal ions, which were obtained using $[Re^{II}(triphos)(CN)_3]^-$ [triphos = 1,1,1-tris(diphenylphosphinoethyl)methane] as a ligand;[7] (iii) recently the redox-switchable SMM $[(PY5Me_2)_4Mn^{II}_4Re^{IV}(CN)_7](PF_6)_5\cdot 6H_2O$ ($PY5Me_2$ = 2,6-bis[1,1-bis(2-pyridyl)ethyl]pyridine).[8]

In this context, a line of our current research work in molecular magnetism has focused on the magnetostructural study of heterometallic compounds containing Re^{IV} and paramagnetic 3d ions where the stable mononuclear complex $[ReCl_4(ox)]^{2-}$ is used as a ligand.[9] Re^{IV} is a $5d^3$ ion, which usually forms octahedral complexes that are reluctant to ligand substitution and are reasonably stable against redox processes.[10] Its ground electronic state is a $^4A_{2g}$ term with three unpaired electrons and a high value of the spin−orbit constant (λ being ca. 1000 cm^{-1} for the free ion). This last fact accounts for the high magnetic anisotropy that Re^{IV} shows.[9a] These features, together with the well-known capability of the oxalate ligand to transmit electronic interactions between paramagnetic metal ions that it connects,[11] make the mononuclear complex $[ReCl_4(ox)]^{2-}$ a very suitable candidate for generating new anisotropic heterometallic magnetic systems. The greater diffuseness of the 5d orbitals is another factor to be taken into account because of the predicted enhancement of the magnetic coupling associated with it. The greater values of the ferromagnetic coupling between Re^{IV} ($5d^3$) and Ni^{II} ($3d^8$) in the dinuclear $[Re^{IV}Cl_4(\mu\text{-ox})Ni^{II}(dmphen)_2]$ (dmphen = 2,9-dimethyl-1,10-phenanthroline; $J = +11.8$ cm^{-1})[9c] and trinuclear $(NBu_4)_2[\{Re^{IV}Cl_4(\mu\text{-ox})\}_2Ni^{II}(Him)_2]$ (Him = imidazole; $J = +14.2$ cm^{-1})[9d] complexes when compared to that observed between Cr^{III} ($3d^3$) and Ni^{II} ($3d^8$) in the tetranuclear compound $[\{Ni(Me_6[14]ane\text{-}N_4)\}_3(\mu\text{-ox})_3Cr](ClO_4)_3$ ($Me_6[14]ane\text{-}N_4$ = (±)-5,7,7,12,14,14-hexamethyl-4,8,11-tetraazacyclotetradecane; $J = +5.3$ cm^{-1})[12] are in agreement with this prediction.

A previous communication on the preparation, crystal structure, and preliminary magnetic study of the tetranuclear complex $(NBu_4)_4[\{ReCl_4(\mu\text{-ox})\}_3Ni^{II}]$ showed this compound to be the first example of a Re^{IV} compound showing SMM behavior and a fast tunneling relaxation process at $H = 0$.[13] Aiming at completing this preliminary study, we present here a detailed magnetostructural investigation on the heterotetranuclear compounds of the general formula $(NBu_4)_4[\{Re^{IV}Cl_4(\mu\text{-ox})\}_3M^{II}]$ [M = Mn (**1**), Fe (**2**), Co (**3**), Ni (**4**), and Cu (**5**)]

(4) (a) Osa, S.; Kido, T.; Matsumoto, N.; Re, N.; Pochaba, A.; Mrozinski, J. *J. Am. Chem. Soc.* **2004**, *126*, 420. (b) Zaleski, F. C. M.; Depperman, E. C.; Kampf, J. W.; Lirk, M. L.; Pecoraro, V. L. *Angew. Chem., Int. Ed.* **2004**, *43*, 3912. (c) Mishra, A.; Wernsdorfer, W.; Abboud, K. A.; Christou, G. *J. Am. Chem. Soc.* **2004**, *126*, 15648. (d) Mishra, A.; Wernsdorfer, W.; Parsons, S.; Christou, G.; Brechin, E. K. *Chem. Commun.* **2005**, 2086. (e) Yukawa, Y.; Aromí, G.; Igarashi, S.; Ribas, J.; Zvyagin, S. A.; Krzystek, J. *Angew. Chem., Int. Ed.* **2005**, *44*, 1997. (f) Costes, J. P.; Auchel, M.; Dahan, F.; Peyrou, V.; Shova, S.; Wernsdorfer, W. *Inorg. Chem.* **2006**, *45*, 1924. (g) Mori, F.; Nyui, T.; Ishida, T.; Nogami, T.; Choi, K. Y.; Nojiri, H. *J. Am. Chem. Soc.* **2006**, *128*, 1440. (h) Aronica, C.; Pilet, G.; Chastanet, G.; Wernsdorfer, W.; Jacquot, J. F.; Luneau, D. *Angew. Chem., Int. Ed.* **2006**, *45*, 4659. (i) Ferbinteanu, M.; Kajiwara, T.; Choi, K.-Y.; Nojiri, H.; Nakamoto, A.; Kojima, N.; Cimpoesu, F.; Fujimura, Y.; Takaishi, S.; Yamashita, M. *J. Am. Chem. Soc.* **2006**, *128*, 9008. (j) Mori, F.; Ishida, T.; Nogami, T. *Polyhedron* **2006**, *24*, 2588. (k) Murugesu, M.; Mishra, A.; Wernsdorfer, W.; Abboud, K. A.; Christou, G. *Polyhedron* **2006**, *25*, 613. (l) Pointillart, F.; Bernot, K.; Sessoli, R.; Gatteschi, D. *Chem.—Eur. J.* **2007**, *13*, 1602. (m) Mereacre, V. M.; Ako, A. M.; Clérac, R.; Wernsdorfer, W.; Filoti, G.; Bartolome, J.; Anson, C. E.; Powell, A. K. *J. Am. Chem. Soc.* **2007**, *129*, 9248. (n) Zaleski, C. M.; Kampf, J. W.; Mallah, T.; Kirk, M. L.; Pecoraro, V. L. *Inorg. Chem.* **2007**, *46*, 1954. (o) Mishra, A.; Tasiopoulos, A. J.; Wernsdorfer, W.; Abboud, K. A.; Christou, G. *Inorg. Chem.* **2007**, *46*, 3105. (p) Hamamatsu, T.; Yabe, K.; Towatari, M.; Osa, S.; Matsumoto, N.; Re, N.; Pochaba, A.; Mrozinski, J.; Gallani, J. L.; Barla, A.; Imperia, P.; Paulsen, C.; Kappler, J. P. *Inorg. Chem.* **2007**, *46*, 4458. (q) Mereacre, V.; Ako, A. M.; Clérac, R.; Wernsdorfer, W.; Hewitt, I. J.; Anson, C. E.; Powell, A. K. *Chem.—Eur. J.* **2008**, *14*, 3577. (r) Chandrasekhar, V.; Pandian, B. M.; Boomishankar, R.; Steiner, A.; Vittal, J. J.; Houri, A.; Clérac, R. *Inorg. Chem.* **2008**, *47*, 4918.

(5) (a) Ishikawa, N.; Sugita, M.; Ishikawa, T.; Koshihara, S.; Kaizu, Y. *J. Am. Chem. Soc.* **2003**, *125*, 8694. (b) Ishikawa, N.; Sugita, M.; Wernsdorfer, W. *Angew. Chem., Int. Ed.* **2005**, *44*, 2.

(6) Sokol, J. J.; Hee, A. G.; Long, J. R. *J. Am. Chem. Soc.* **2002**, *124*, 7656.

(7) (a) Schelter, E. J.; Prosvirin, A. V.; Reiff, W. M.; Dunbar, K. R. *Angew. Chem., Int. Ed.* **2004**, *43*, 4912. (b) Schelter, E. J.; Prosvirin, A. V.; Dunbar, K. R. *J. Am. Chem. Soc.* **2004**, *126*, 15004. (c) Schelter, E. J.; Karadas, F.; Avendano, C.; Prosvirin, A. V.; Wernsdorfer, W.; Dunbar, K. R. *J. Am. Chem. Soc.* **2007**, *129*, 8139.

(8) Freedman, D. E.; Jenkins, D. M.; Lavarone, A. T.; Long, J. R. *J. Am. Chem. Soc.* **2008**, *130*, 2884.

(9) (a) Chiozzone, R.; González, R.; Kremer, C.; De Munno, G.; Cano, J.; Lloret, F.; Julve, M.; Faus, J. *Inorg. Chem.* **1999**, *38*, 4745. (b) Chiozzone, R.; González, R.; Kremer, C.; De Munno, G.; Armentano, D.; Cano, J.; Lloret, F.; Julve, M.; Faus, J. *Inorg. Chem.* **2001**, *40*, 4242. (c) Chiozzone, R.; González, R.; Kremer, C.; De Munno, G.; Armentano, D.; Lloret, F.; Julve, M.; Faus, J. *Inorg. Chem.* **2003**, *42*, 1064. (d) Martínez-Lillo, J.; Delgado, F. S.; Ruiz-Pérez, C.; Lloret, F.; Julve, M.; Faus, J. *Inorg. Chem.* **2007**, *46*, 3523. (e) Martínez-Lillo, J.; Armentano, D.; De Munno, G.; Lloret, F.; Julve, M.; Faus, J. *Dalton Trans.* **2008**, 40.

(10) (a) Rouschias, G. *Chem. Rev.* **1974**, *74*, 531. (b) Conner, K. A.; Walton, R. A. In *Comprehensive Coordination Chemistry*; Wilkinson, G., Gillard, R. D., McCleverty, J. A., Eds.; Pergamon Press: New York, 1987; Vol. *4*, p 165.

(11) (a) Julve, M.; Verdaguer, M.; Kahn, O.; Gleizes, A.; Philoche-Levisalles, M. *Inorg. Chem.* **1983**, *22*, 370. (b) Julve, M.; Verdaguer, M.; Gleizes, A.; Philoche-Levisalles, M.; Kahn, O. *Inorg. Chem.* **1984**, *23*, 3808. (c) Julve, M.; Faus, J.; Verdaguer, M.; Gleizes, A. *J. Am. Chem. Soc.* **1984**, *106*, 8306. (d) Alvarez, S.; Julve, M.; Verdaguer, M. *Inorg. Chem.* **1990**, *29*, 4500. (e) Gleizes, A.; Julve, M.; Verdaguer, M.; Real, J. A.; Faus, J.; Solans, X. *J. Chem. Soc., Dalton Trans.* **1992**, 3209. (f) Cano, J.; Alemany, P.; Alvarez, S.; Verdaguer, M.; Ruiz, E. *Chem.—Eur. J.* **1998**, *4*, 476.

(12) Pei, Y.; Journaux, Y.; Kahn, O. *Inorg. Chem.* **1983**, *22*, 2624.

(13) Martínez-Lillo, J.; Armentano, D.; De Munno, G.; Wernsdorfer, W.; Julve, M.; Lloret, F.; Faus, J. *J. Am. Chem. Soc.* **2006**, *128*, 14218.

where intramolecular antiferromagnetic (**1**) and ferromagnetic couplings (**2**−**5**) occur.

Experimental Section

Materials. All starting chemicals and solvents were purchased from commercial sources and used without further purification. The mononuclear precursor $(NBu_4)_2[ReCl_4(ox)]$ was prepared following the procedure described for $(AsPh_4)_2[ReCl_4(ox)]$ by using NBu_4Cl instead of $AsPh_4Cl$ as the precipitating agent.[14]

Synthesis of the Complexes. $(NBu_4)_4[\{ReCl_4(\mu\text{-ox})\}_3Mn]$ (1). A solution of 67.5 mg (0.075 mmol) of $(NBu_4)_2[ReCl_4(ox)]$ in a 2-propanol/MeCN (10:1, v/v) mixture (30 mL) was added to a solution of 6.3 mg (0.025 mmol) of $Mn(NO_3)_2\cdot 4H_2O$ in 30 mL of 2-propanol under continuous stirring. The resulting yellowish-green solution was allowed to evaporate in an argon atmosphere at room temperature. **1** was formed as a fine green solid in 2 weeks. It was filtered off and washed with cold 2-propanol and diethyl ether. The obtained solid poorly diffracts. All of our efforts to grow X-ray-quality crystals were unsuccessful, including modification of the Re/M molar ratio in the synthesis, which works with the Fe and Cu complexes (vide infra). Yield: ca. 65%. Anal. Calcd for $C_{70}H_{144}N_4Cl_{12}O_{12}MnRe_3$ (**1**): C, 36.80; H, 6.40; N, 2.49. Found: C, 37.06; H, 6.67; N, 2.54. IR/cm^{-1}: bands associated with the oxalato ligand appear at 1680sh, 1655vs, and 809s.

$(NBu_4)_4[\{ReCl_4(\mu\text{-ox})\}_3Fe]$ (2). The preparation of **2** is analogous to that of **1** but using $FeCl_2\cdot 4H_2O$ (5.0 mg, 0.025 mmol) instead of $Mn(NO_3)_2\cdot 4H_2O$. The resulting deep yellow solution is allowed to evaporate slowly in an argon atmosphere. A first crop of an orange solid of **2** separated after a few days. It was filtered off and washed with cold 2-propanol and diethyl ether. Brownish-orange parallelepipeds of **2** suitable for X-ray diffraction were grown from the mother liquor after 2−3 weeks. The best X-ray-quality crystals were obtained when a 1:1 Re/Fe molar ratio was used in the synthesis. Yield: ca. 85%. Anal. Calcd for $C_{70}H_{144}N_4Cl_{12}O_{12}FeRe_3$ (**2**): C, 36.98; H, 6.38; N, 2.46. Found: C, 37.01; H, 6.47; N, 2.45. IR/cm^{-1}: bands associated with the oxalato ligand appear at 1656vs and 808s.

$(NBu_4)_4[\{ReCl_4(\mu\text{-ox})\}_3Co]$ (3). This complex was prepared by using the same procedure as that described for **1** but replacing $Mn(NO_3)_2\cdot 4H_2O$ with $Co(NO_3)_2\cdot 6H_2O$ (14.6 mg, 0.05 mmol). The resulting pale-yellow solution was allowed to evaporate slowly in an argon atmosphere at room temperature. Pink parallelepipeds of **3** were obtained after 1.5 months. They were collected by filtration and washed with cold 2-propanol and diethyl ether. Yield: ca. 70%. Anal. Calcd for $C_{70}H_{144}N_4Cl_{12}O_{12}CoRe_3$ (**3**): C, 36.93; H, 6.37; N, 2.46. Found: C, 36.80; H, 6.60; N, 2.50. IR/cm^{-1}: bands associated with the oxalato ligand appear at 1649vs and 812s.

$(NBu_4)_4[\{ReCl_4(\mu\text{-ox})\}_3Ni]$ (4). A solution of 67.5 mg (0.075 mmol) of $(NBu_4)_2[ReCl_4(ox)]$ in a 2-propanol/MeCN mixture (10:1, v/v; 30 mL) was poured into a solution of 7.4 mg (0.025 mmol) of $Ni(NO_3)_2\cdot 6H_2O$ in 30 mL of 2-propanol, leading to a pale-green solution. Suitable X-ray-quality crystals of **4** as green parallelepipeds were separated from the mother liquor after 2−3 weeks by slow evaporation in the open air at room temperature. The crystals of **4** were filtered off and washed with cold 2-propanol and diethyl ether. Yield: ca. 86%. Anal. Calcd for $C_{70}H_{144}N_4Cl_{12}O_{12}NiRe_3$ (**4**): C, 36.93; H, 6.38; N, 2.46. Found: C, 36.78; H, 6.62; N, 2.51. IR/cm^{-1}: bands associated with the oxalato ligand appear at 1680sh, 1650vs, and 809s.

$(NBu_4)_4[\{ReCl_4(\mu\text{-ox})\}_3Cu]$ (5). The preparation of complex **5** follows that of **4** but using the copper(II) nitrate trihydrate (6.1 mg, 0.025 mmol) instead of $Ni(NO_3)_2\cdot 6H_2O$. The resulting yellowish-green solution was allowed to slow evaporation in the open air at room temperature. Yellow parallelepipeds of **5** were obtained after 1 week. They were collected by filtration and washed with cold 2-propanol and diethyl ether. The best X-ray-quality crystals of **5** were obtained when a 1:1 Re/Cu molar ratio was used in the synthesis. Yield: ca. 70%. Anal. Calcd for $C_{70}H_{144}N_4Cl_{12}O_{12}CuRe_3$ (**5**): C, 36.85; H, 6.36; N, 2.46. Found: C, 36.81; H, 6.78; N, 2.47. IR/cm^{-1}: bands associated with the oxalato ligand are located at 1682m, 1650vs, and 807s. The absence of the ca. 1680 cm^{-1} feature in the IR spectra of **2** and **3**, probably due to the lack of resolution of the bands, is not indicative of a different coordination mode of the oxalato ligand in these compounds, as shown by the X-ray structures.

Physical Measurements. Elemental analyses (C, H, and N) were performed on a CE Instruments EA 1110 CHNS analyzer, and a 3:1 Re/M [M = Mn (**1**), Fe (**2**), Co (**3**), Ni (**4**), and Cu (**5**)] molar ratio was determined by means of a Philips XL-30 scanning electron microscope equipped with an X-ray microanalysis system from the Central Service for the Support to Experimental Research of the Universitat de València. IR spectra were recorded with a Nicolet 320 FT-IR spectrophotometer as KBr pellets in the 4000−400 cm^{-1} region. Magnetic measurements on polycrystalline samples of **1**−**5** were carried out with a Quantum Design SQUID magnetometer in the temperature range 1.9−300 K. Magnetization data were collected in the 0−5 T range starting at zero field at 2.0 K. Alternating current (ac) magnetic susceptibility measurements were performed with an oscillating field of 1 G and in an operating frequency range of 1−1400 Hz. Diamagnetic corrections of the constituent atoms were estimated from Pascal's constants.[15] Micro-SQUID measurements were collected on a sample of aligned single crystals of **4** in the temperature range from 0.04 to 7 K and in fields of up to 1.4 T.[16] The field can be applied in any direction of the micro-SQUID plane with a precision much better than 0.1° by separately driving three orthogonal superconducting coils. The field was aligned with the easy axis of magnetization by using the transverse field method.[16b] High-frequency electron paramagnetic resonance (HFEPR) spectra were recorded on a polycrystalline sample of **4** (ca. 18 mg) at multiple frequencies using all of the subterahertz wave sources available at the NHMFL, covering quasi-continuously the range of 50−700 GHz, in conjunction with a 15/17-T superconducting magnet. Detection was provided with an InSb hot electron bolometer (QMC Ltd., Cardiff, U.K.). The magnetic field was modulated at 10 kHz for detection purposes. A Standford Research Systems SR830 lock-in amplifier converted the modulated signal to direct current voltage.

Crystallographic Data Collection and Structure Determination. Diffraction data of **2**−**5** were collected with a Bruker-Nonius X8 APEX II CCD area detector diffractometer, using monochromatized Mo Kα radiation (λ = 0.710 73 Å). A total of 3908 (**2**), 4032 (**3**), 2175 (**4**), and 1043 (**5**) frames of data were collected using a narrow-frame method with scan widths of 0.3° in ϕ and ω with exposure times of 10 s (**2** and **4**) and 30 s (**3** and **5**) per frame using crystal-to-detector distances of 50 mm (**2** and **4**) and 40 mm

(14) (a) Chiozzone, R.; Cuevas, A.; González, R.; Kremer, C.; Armentano, D.; De Munno, G.; Faus, J. *Inorg. Chim. Acta* **2006**, *359*, 2194. (b) Tomkiewicz, A.; Bartczak, T. J.; Kruszynski, R.; Mrozinski, J. *J. Mol. Struct.* **2001**, *595*, 225.

(15) Earnshaw, A. *Introduction to Magnetochemistry*; Academic Press: London, 1968.

(16) (a) Wernsdorfer, W. *Adv. Chem. Phys.* **2001**, *118*, 99. (b) Wernsdorfer, W.; Chakov, N. E.; Christou, G. *Phys. Rev. B* **2004**, *70*, 132413.

Table 1. Crystallographic Data for $(NBu_4)_4[\{ReCl_4(\mu\text{-ox})\}_3M]$ with M = Fe (**2**), Co (**3**), Ni (**4**), and Cu (**5**)

	2	**3**	**4**	**5**
formula	$C_{70}H_{144}Cl_{12}N_4O_{12}Re_3Fe$	$C_{70}H_{144}Cl_{12}N_4O_{12}Re_3Co$	$C_{70}H_{144}Cl_{12}N_4O_{12}Re_3Ni$	$C_{70}H_{144}Cl_{12}N_4O_{12}Re_3Cu$
fw	2273.74	2276.82	2276.60	2281.43
cryst syst	triclinic	triclinic	triclinic	triclinic
space group	$P\bar{1}$	$P\bar{1}$	$P\bar{1}$	$P\bar{1}$
a/Å	10.005(1)	10.216(1)	10.229(1)	10.046(1)
b/Å	19.468(2)	16.950(1)	16.975(1)	19.328(4)
c/Å	25.580(2)	30.772(2)	30.800(1)	25.511(5)
α/deg	83.783(3)	76.097(3)	76.139(1)	83.913(5)
β/deg	83.403(3)	80.944(3)	80.669(2)	83.705(6)
γ/deg	80.960(3)	78.508(3)	78.504(2)	80.444(5)
V/Å^3	4867.2(7)	5035.2(5)	5051.1(3)	4835.9(15)
Z	2	2	2	2
T/K	296(2)	296(2)	296(2)	298(2)
D_c/g cm^{-3}	1.551	1.502	1.497	1.567
F(000)	2286	2288	2290	2292
μ(Mo Kα)/mm^{-1}	4.244	4.123	4.133	4.342
rflns colld	97 090	62 707	46 364	29 643
rflns indep (R_{int})	20 920 (0.0327)	10 537 (0.0512)	21 221 (0.0308)	9867 (0.0647)
R1[a] [$I > 2(I)$] (all)	0.0481 (0.0717)	0.0494 (0.0733)	0.0508 (0.0949)	0.0604 (0.0998)
wR2[b] [$I > 2(I)$] (all)	0.1332 (0.1536)	0.1498 (0.1770)	0.1352 (0.1731)	0.1524 (0.1891)
GOF on F^2	1.063	1.088	0.963	1.035

[a] $R1 = (||F_o| - |F_c||)/|F_o|$. [b] $wR2 = \{[w(F_o^2 - F_c^2)^2]/[w(F_o^2)^2]\}^{1/2}$.

(**3** and **5**). The unit cell parameters were based upon least-squares refinement of 7634 (**2**), 9457 (**3**), 7859 (**4**), and 3041 (**5**) reflections. Data collection was carried out in the ranges $0.80° > \theta > 26.99°$ (**2**), $0.69° > \theta > 21.02°$ (**3**), $0.69° > \theta > 26.80°$ (**4**), and $0.81° > \theta > 20.78°$ (**5**), and their processing was done through the *SAINT*[17] reduction and *SADABS*[18] absorption software. Unfortunately, crystals of **3** and **5** are too small and of low quality, diffracting very poorly at $\theta > 21°$. All attempts to grow higher-X-ray-quality crystals to allow a better structure determination failed. Of the 97 090 (**2**), 62 707 (**3**), 46 364 (**4**), and 29 643 (**5**) collected reflections, 20 920 (**2**), 10 537 (**3**), 21 221 (**4**), and 9867 (**5**) of them were unique [$I < 2\sigma(I)$] and were used for refinement of the structures. The structures of **2**−**5** were solved by direct methods and subsequently completed by Fourier recycling using the *SHELXTL* software package.[19] All non-H atoms of the tetranuclear entity of **2**−**5** were refined anisotropically. Considering the *n*-butyl side chains, they are affected by a large thermal motion and the more physically reasonable models have been developed. In particular, the refinement in compounds **2** and **4** was done with the C(57) and C(58) (**2**) and C(66) (**4**) carbon atoms fixed as obtained from the ΔF map, and they were not refined. The non-H atoms of the tetra-*n*-butylammonium cation in **3** and **5** were refined isotropically to increase the low reflections/parameters ratio. All H atoms in **2**−**5** were set in calculated positions and refined as riding atoms.

Full-matrix least-squares refinements on F^2 for **2**−**5** were carried out by minimizing the function $\sum w(|F_o| - |F_c|)^2$, and they reached convergence with values of the discrepancy indices given in Table 1. The final geometrical calculations were carried out with the *PARST97*[20a] program, whereas the graphical manipulations were performed with the *CRYSTALMAKER*[20b] program and the XP utility of the *SHELXTL* system. Selected bond lengths and angles for **2**−**5** are listed in Table S1 in the Supporting Information.

Results and Discussion

Description of the Crystal Structures. The crystal structures of compounds **2**−**5** are made up of $[\{Re^{IV}Cl_4(ox)\}_3M^{II}]^{4-}$ anions [M = Fe (**2**), Co (**3**), Ni (**4**), and Cu (**5**)] and $[n\text{-}(C_4H_9)_4N]^+$ cations, which are held together by electrostatic forces. **2** and **5** are isostructural compounds, as are **3** and **4**. A perspective drawing of the structure of the tetranuclear entity of **2** showing the atom numbering is depicted in Figure 1. Identical atom numbering has been adopted for the corresponding units of **3**−**5** (Figures S1−S3 in the Supporting Information). The main difference between the whole structures of **2** and **5** with respect to **3** and **4** is in the overall packing, which leads to greater anion−anion separations through the bulky tetra-*n*-butylammonium cations in **3** and **4** with respect to those in **2** and **5** [Figures S4 (**2** and **5**) and S5 (**3** and **4**) in the Supporting Information], as shown by the values of the shortest intermolecular distances Re···Re [8.300(1) (**2**), 9.759(1) (**3**), 9.803(1) (**4**), and 8.361(1) Å (**5**)] and Cl···Cl [3.758(1) (**2**), 5.588(1) (**3**), 5.608(1) (**4**), and 3.838(1) Å (**5**)], with the latter ones being beyond the sum of the van der Waals radii (ca. 3.60 Å).

Each $[\{ReCl_4(ox)\}_3M]^{4-}$ unit in **2**−**5** contains three peripheral Re atoms and one central M atom, which are interconnected through three bis-bidentate oxalate ligands. The four M atoms of this entity are coplanar. Each Re atom is surrounded by two oxalate O atoms and four chloride anions in a distorted octahedral geometry. The short bite angle of the oxalato is the main cause of the distortion, with the value of the angle subtended by this ligand at the Re atom varying in the range 77.6(4)−80.2(3)°. No significant differences were found in the Re−Cl [values covering the range 2.266(5)−2.352(5) Å] and Re−O [minimum and maximum values being 2.032(10) and 2.097(4) Å, respectively] bond lengths in this series of compounds. The bond lengths and angles within the $[ReCl_4(ox)]$ fragment are in agreement with those found for this unit in previous reports.[9] The best equatorial plane around the Re atoms is defined by the O(3)−O(4)−Cl(2)−Cl(3) [at Re(1)], O(7)−O(8)−Cl(6)−Cl(7) [at Re(2)], and O(10)−O(11)−Cl(10)−Cl(11) [at Re(3)] sets of atoms, with the value of the largest deviation from the mean plane being 0.064(5) Å at O(1) in

(17) *SAINT*, version 6.45; Bruker Analytical X-ray Systems: Madison, WI, 2003.
(18) Sheldrick G. M. *SADABS Program for Absorption Correction*, version 2.10; Analytical X-ray Systems: Madison, WI, 2003.
(19) *SHELXTL*; Bruker Analytical X-ray Instruments: Madison, WI, 1998.

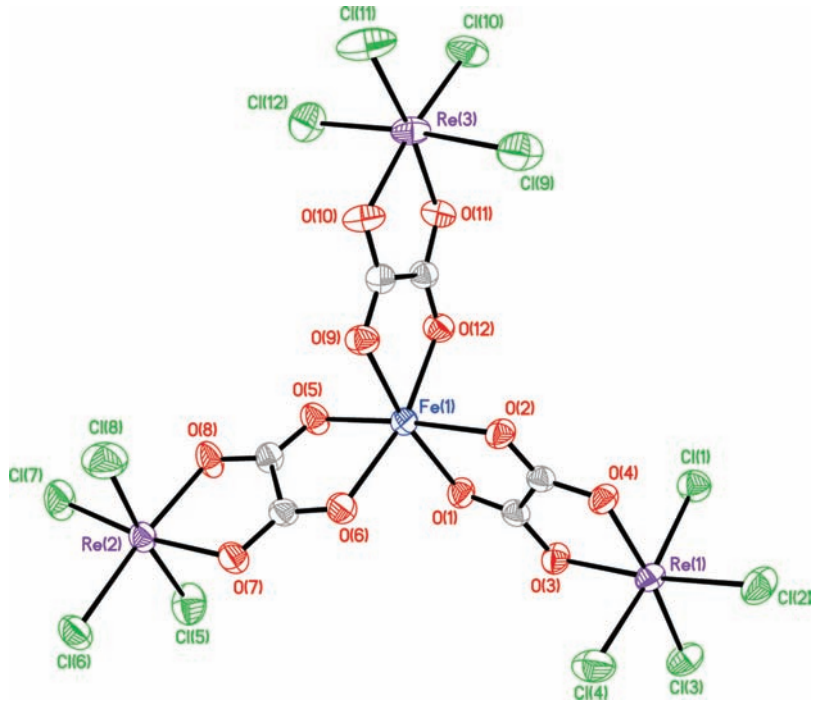

Figure 1. Perspective view of the heterotetranuclear $[M^{II}\{ReCl_4(\mu\text{-ox})\}_3]^{4-}$ unit in **2** (M = Fe) with the atom numbering of metal chromophores. The thermal ellipsoids are drawn at the 30% probability level.

5. The Re atoms lie in the respective equatorial planes in the four complexes. The values of the dihedral angles between each equatorial plane and the respective oxalate group vary in the ranges 2.6−6.3° (**2**), 2.5−3.7° (**3**), 2.4−3.0° (**4**), and 1.7−6.7° (**5**).

The M atoms are also six-coordinated, with six oxalate O atoms from three $[ReCl_4(ox)]^{2-}$ units building somewhat distorted octahedral surroundings. As observed for the Re atom, the main source of distortion of the ideal octahedral geometry at the M atom is due to the reduced bite angle of the oxalato [the values of the O(1)−M(1)−O(2), O(5)−M(1)−O(6), and O(9)−M(1)−O(12) angles varying in the ranges 78.8(1)−82.2(4)°, 78.42(14)−81.97(18)°, and 77.8(4)−82.42(17)°, respectively]. The values of the M−O(ox) lengths in **2**−**5** are close to those observed for other oxalato-bridged Re^{IV}−M^{II} complexes.[9c,d] The values of the Re···M separation across the bridging oxalate are 5.484(1) (**2**), 5.430(1) (**3**), 5.351(1) (**4**), and 5.565(2) (**5**) Å. The degree of twist (ϕ) of the trischelated environment of the M atom is 49° (**4**), 59° (**3**), and 60° (**2** and **5**) (ϕ = 60° for a regular octahedron).[21]

The oxalate groups are practically planar, and their bond lengths and angles are as expected. The values of the dihedral angles between their mean planes in each trischelated $M(ox)_3$ fragment cover the ranges 84.7−91.6° (**2**), 75.0−93.6° (**3**), 77.2−91.0° (**4**), and 85.4−91.1° (**5**). The bond lengths and angles of each tetrahedral $[n\text{-}(C_4H_9)_4N]^+$ cation in **2**−**5** are normal and do not require any comment.[22] The scatter in the N−C and C−C distances and in the N−C−C and C−C−C angles doubtless arises from the considerable thermal motion, which is quite a common feature of $[n\text{-}(C_4H_9)_4N]^+$ in most of the compounds containing this cation.

Magnetic Properties of 1−5. For pedagogic reasons, we will describe and analyze the magnetic properties of this family of complexes following the increasing number of unpaired electrons of the M^{II} cation. Because of the SMM-like behavior observed for **4**, a thorough magnetic study (ac, HFEPR, and micro-SQUID measurements) on this compound is provided in a new paragraph after the description, analysis, and discussion of the magnetic properties of **1**−**5** [see Figures 2 (**5**), 3 (**4**), 4 (**3**), 5 (**2**), and 6 (**1**), where χ_M is the magnetic susceptibility per $Re^{IV}{}_3M^{II}$ unit].

Because of the complexity of the magnetic analysis of the $Re^{IV}{}_3M^{II}$ series and given that the $[ReCl_4(ox)]^{2-}$ unit is present in this family, it seems convenient to reiterate briefly the magnetic behavior of such a Re^{IV} unit when it is magnetically isolated. The value of $\chi_M T$ at room temperature for such a unit is ca. 1.60 $cm^3\ mol^{-1}\ K$ (per 1 mol of the Re atom) with $S_{Re} = {}^3/_2$ and $g_{Re} = 1.8-1.9$.[9a] When cooling, the value of $\chi_M T$ for this magnetically isolated unit decreases because of the zfs effects ($2D_{Re}$, that is, the energy gap between the $M_S = \pm{}^3/_2$ and $\pm{}^1/_2$ Kramers doublets) resulting from the combined action of the second-order spin−orbit interaction and the tetragonal field of the six-coordinated Re^{IV} ion. The high value of the spin−orbit coupling constant for Re^{IV}, a third-row transition-metal ion with λ of ca. 1000

(20) (a) Nardelli, M. *J. Appl. Crystallogr.* **1995**, *28*, 659. (b) *CRYSTALMAKER*, version 6.3.1; CambridgeSoft Corp.: Oxfordshire, U.K., 2003.
(21) Kepert, D. L. *Prog. Inorg. Chem.* **1977**, *23*, 1.
(22) (a) Atovmyan, L. O.; Shilov, G. V.; Lyubovskaya, R. N.; Zhilyaeva, E. I.; Ovanesyan, N. S.; Pirumova, S. I.; Gusakovskaya, I. G.; Morozov, Y. G. *JEPT Lett.* **1993**, *58*, 766. (b) Mathonière, C.; Nuttall, J.; Carling, S. G.; Day, P. *Inorg. Chem.* **1996**, *35*, 1201. (c) Pellaux, R.; Schmalle, H. W.; Huber, R.; Fischer, P.; Hauss, T.; Ouladdiaf, B.; Decurtins, S. *Inorg. Chem.* **1997**, *36*, 2301. (d) Watts, I. D.; Carling, S. G.; Day, P. *J. Chem. Soc., Dalton Trans.* **2002**, 1429.

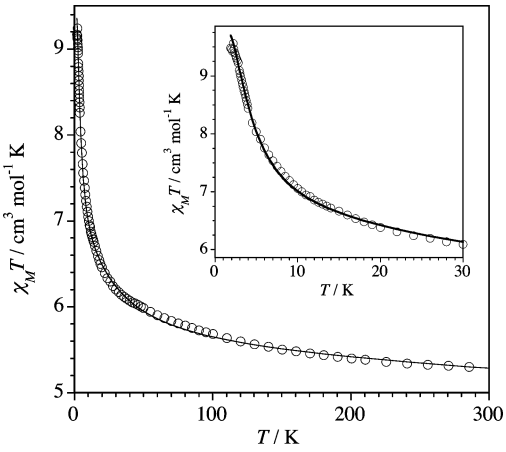

Figure 2. Thermal variation of the $\chi_M T$ product for **5** under an applied magnetic field of 250 G: (○) experimental data; (—) best-fit curve (see the text). The inset shows details of the low-temperature region.

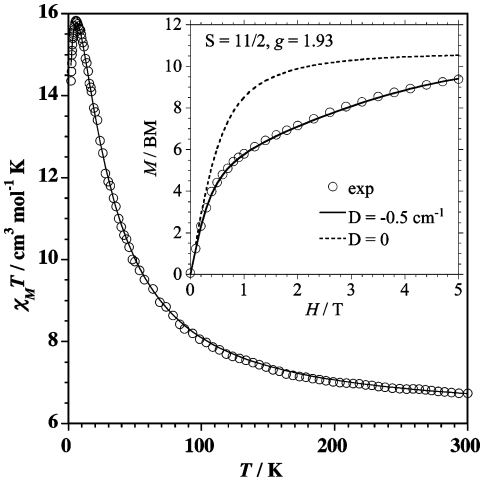

Figure 3. Thermal variation of the $\chi_M T$ product for **4** under an applied magnetic field of 100 G: (○) experimental data; (—) best-fit curve (see the text). The inset shows the magnetization vs H plot at 2.0 K: (○) experimental data; theoretical curves for $S = {}^{11}/_2$ and $g = 1.93$ with $D_{11/2} = 0$ (- - -) and $-0.50(1)$ cm^{-1} (—).

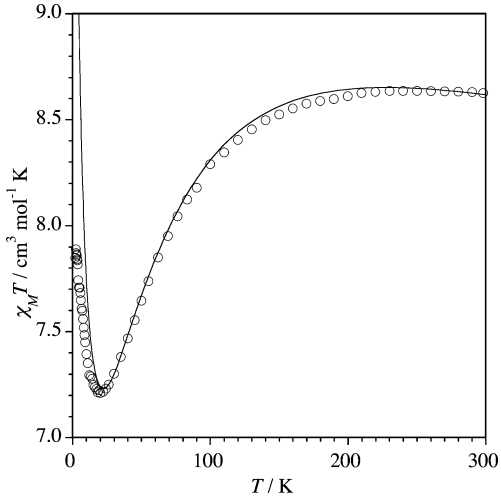

Figure 4. Thermal variation of the $\chi_M T$ product for **3** under an applied magnetic field of 100 G: (○) experimental data; (—) best-fit curve (see the text).

cm^{-1}in the free ion, leads to large values of the zero-field splitting (values up to 50 cm^{-1}).[9] In the low-temperature

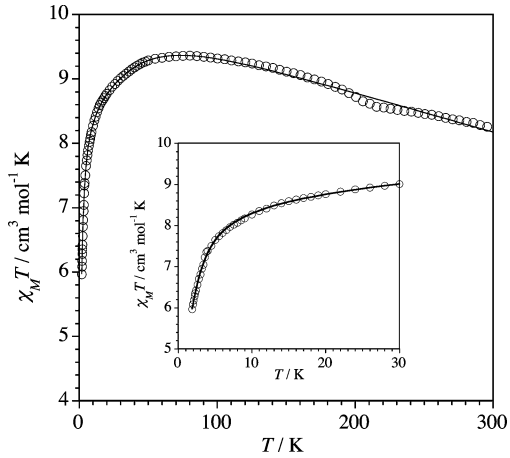

Figure 5. Thermal variation of the $\chi_M T$ product for **2** under an applied magnetic field of 100 G: (○) experimental data; (—) best-fit curve (see the text). The inset shows details of the low-temperature region.

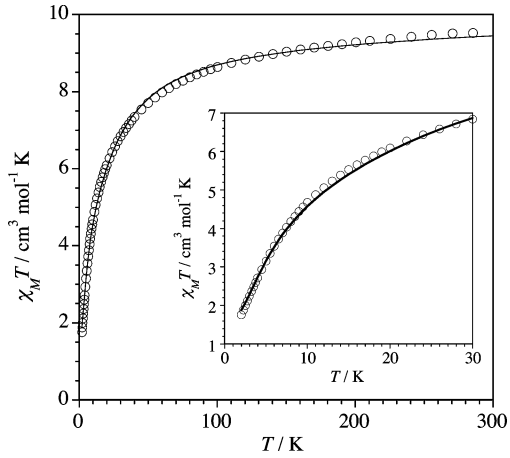

Figure 6. Thermal variation of the $\chi_M T$ product for **1** under an applied magnetic field of 250 G: (○) experimental data; (—) best-fit curve (see the text). The inset shows details of the low-temperature region.

region where $kT \ll |2D_{Re}|$, this entity can be viewed as an Ising spin $S = {}^1/_2$ system[23] with $\chi_{av}T$ of ca. 1.0 cm^3 mol^{-1} K (χ_{av} being the average powder susceptibility with $g = g_{\parallel} = g_{\perp}$).

The value of $\chi_M T$ for **5** at room temperature is 5.28 cm^3 mol^{-1} K (Figure 2), as expected for one Cu^{II} ($\chi_M T = 0.41$ cm^3 mol^{-1} K with $S_{Cu} = {}^1/_2$ and $g_{Cu} = 2.1$) and three Re^{IV} magnetically noninteracting ($\chi_M T = 3 \times 1.6 + 0.40 = 5.20$ cm^3 mol^{-1} K; see above). This value continuously increases upon cooling, and it attains a maximum value of 9.25 cm^3 mol^{-1} K at 1.9 K. The shape of this curve unambiguously supports the occurrence of a significant ferromagnetic interaction between the peripheral Re^{IV} ions and the central Cu^{II} through the oxalato bridge. In light of the tetranuclear structure of **5** and the above specified magnetic considerations, we have analyzed its magnetic data through the general Hamiltonian of eq 1, which will be applied to the different systems reported herein

(23) Ising, E. *Z. Phys.* **1925**, *31*, 253.

$$\hat{H} = \hat{H}_{exchange} + \hat{H}_{zfs} + \hat{H}_{Zeeman}$$
$$\hat{H}_{exchange} = -J_{ReM}\hat{S}_M \sum_{i=1}^{3} \hat{S}_{Rei}$$
$$\hat{H}_{zfs} = D_{Re} \sum_{i=1}^{3} \left(\hat{S}_{ZRei}{}^2 - \frac{15}{4}\right) + D_M\left[\hat{S}_{ZM}{}^2 - \frac{n(n+2)}{12}\right]$$
$$\hat{H}_{Zeeman} = g_{Re}^{||}\beta H \sum_{i=1}^{3} \hat{S}_{ZRei} + g_M^{||}\beta H \hat{S}_{ZM} + g_{Re}^{\perp}\beta H \sum_{i=1}^{3} (\hat{S}_{XRei} + \hat{S}_{YRei}) + g_M^{\perp}\beta H(\hat{S}_{XM} + \hat{S}_{YM}) \quad (1)$$

and where J is the exchange-coupling parameter between each peripheral Re^{IV} and the central M^{II} local spins [M = Cu (**5**)], n is the number of unpaired electrons on the M^{II} center ($n = 1$ for **5**), and D_M is the zfs of the M^{II} ions (it is strictly zero for M = Cu). The last term in eq 1 accounts for the Zeeman effects of the four metal ions. In order to reduce the large number of variable parameters and to avoid overparametrization, we have assumed that $g = g_{||} = g_{\perp}$ for the Re^{IV} and Cu^{II} ions. Least-squares fitting of the magnetic data of **5** through eq 1 leads to the parameters listed in Table 2. As one can see in Figure 2, the calculated curve matches very well the experimental data in the whole temperature range explored.

$\chi_M T$ at room temperature for **4** is 6.73 $cm^3\ mol^{-1}$ K (see Figure 3), a value that is as expected for one Ni^{II} ($S_{Ni} = 1$) and three Re^{IV} ions ($S_{Re} = {}^3/_2$) magnetically noninteracting. Upon cooling, $\chi_M T$ continuously increases to reach a maximum value of 15.8 $cm^3\ mol^{-1}$ K at 6.0 K and further decreases to 14.4 $cm^3\ mol^{-1}$ K at 1.9 K. These features are typical of an intramolecular ferromagnetic interaction, with the small decrease of $\chi_M T$ in the very low-temperature range being most likely due to zfs effects. The magnetic data of **4** were analyzed through the Hamiltonian of eq 1 (M = Ni), assuming that the three Re centers are equivalent and $g_{||} = g_{\perp}$ for both Re^{IV} and Ni^{II} ions. Because of the strong correlation observed in the fitting process between the D_{Re} and D_{Ni} parameters, we fix $D_{Ni} = 0\ cm^{-1}$. The corresponding values of the best-fit parameters are listed in Table 2. The good simulation of the susceptibility data for **4** with these parameters supports the occurrence of the $S = {}^{11}/_2$ spin state as the only populated spin state at low temperatures. The corresponding value of $\chi_M T$ for the low-lying $S = {}^{11}/_2$ spin state when fully populated is 16.65 $cm^3\ mol^{-1}$ K with $g_{11/2} = 1.93$. The value of $g_{11/2}$ is computed through the expression $g_{11/2} = 0.819g_{Re} + 0.181g_{Ni}$ with $g_{Re} = 1.87$ and $g_{Ni} = 2.18$ (values of the average Landé factors taken from Table 2), assuming a linear arrangement of the g_{Re} and g_{Ni} local tensors. A value of $|D_{11/2}| = 0.46\ cm^{-1}$ is computed through the expression $D_{11/2} = 0.163D_{Re} + 0.0182D_{Ni}$ by considering that the local **D** tensors are collinear. The computed value of D_{Re} is much smaller than that observed for the magnetically isolated $[ReCl_4(ox)]^{2-}$ anion.[9a] A noncollinear situation of the local **D** tensors would account for this difference. The calculated absolute value of $D_{11/2}$ agrees with that extracted from the magnetization plot at 2.0 K, $D_{11/2} = -0.50\ cm^{-1}$ (inset of Figure 3). Moreover, this value is practically identical with that calculated by using the reduced-field data under different values of the applied dc magnetic field.

Table 2. Best-Fit Parameters for Complexes **1**−**5**

	1	**2**	**3**[a]	**4**	**5**
J, cm^{-1}	−1.30	+1.62	+3.0	+16.3	+4.64
$\|D_{Re}\|$, cm^{-1}	23.1	40.9	45	2.8	14.3
$\|D_M\|$, cm^{-1}	0.00	7.77		0.00	
g_{Re}	1.95(1)	1.89(1)	1.95	1.87	1.93
g_M	2.00(1)	2.30(1)		2.18	2.20
R[b]	4.3×10^{-5}	1.2×10^{-4}	7×10^{-4}	1.6×10^{-5}	2.6×10^{-5}

[a] $\lambda = -150\ cm^{-1}$, $\Delta = -200\ cm^{-1}$, and $\alpha = 1.28$. [b] R is the agreement factor defined as $\sum_i[(\chi_M T)\text{obs}(i) - (\chi_M T)\text{calc}(i)]^2/\sum_i[(\chi_M T)\text{obs}(i)]^2$.

$\chi_M T$ at room temperature for **3** is equal to 8.63 $cm^3\ mol^{-1}$ K (Figure 4), a value that is consistent with the presence of a high-spin Co^{II} ion ($S_{Co} = {}^3/_2$ with unquenched orbital momentum) and three Re^{IV} ions magnetically noninteracting. Upon cooling, $\chi_M T$ smoothly decreases to a minimum value of 7.20 $cm^3\ mol^{-1}$ K at 20.0 K, and it increases further to reach a maximum of 7.88 $cm^3\ mol^{-1}$ K at 2.0 K. These features can be interpreted as follows: the spin−orbit coupling effects of the high-spin Co^{II} ion (depopulation of the higher energy Kramers doublets) and the zfs effects of the three Re^{IV} ions account for the decrease of $\chi_M T$ in the high-temperature range, whereas the further increase of $\chi_M T$ is due to the intramolecular ferromagnetic interaction between the central Co^{II} ions and the peripheral Re^{IV} ions. The occurrence of the ferromagnetic coupling through the bridging oxalato in **3** is supported by the fact that the $\chi_M T$ value at the minimum (ca. 7.20 $cm^3\ mol^{-1}$ K at 20 K) is well above that calculated for a magnetically noninteracting four-spin set of three Re^{IV} and one Co^{II} centers ($\chi_M T$ of ca. 4.7 $cm^3\ mol^{-1}$ K) [one must take into account that $\chi_M T$ for a magnetically isolated Re^{IV} unit tends to a finite value close to 1.0 $cm^3\ mol^{-1}$ K at 1.9 K (see above) and that, at $T < 30$ K, the Co^{II} ion has $S_{eff} = {}^1/_2$ with a g value of ca. 4.2].[24] For the analysis of the magnetic data of **3**, the above Hamiltonian can be applied to metal ions with nondegenerate ground-state terms in an octahedral environment, a condition that is not fulfilled by the six-coordinated high-spin Co^{II}. This cation has a $^4T_{1g}$ ground-state term that is split into a sextet, a quartet, and a Kramers doublet with spin−orbit coupling.[24,25] Moreover, the axially distorted six-coordinated Co^{II} in **3** splits the T term into one doublet and one singlet orbital states. Consequently, the Hamiltonian to analyze the magnetic data of **3** is more complex, and the terms of eqs 2a−2c have to be added to those from the Hamiltonian of eq 1.

$$\hat{H}_{so} = -\alpha\lambda\hat{L}_{Co}\hat{S}_{Co} \quad (2a)$$
$$\hat{H}_{ax} = \Delta\left(\hat{L}_{ZCo^2} - \frac{2}{3}\right) \quad (2b)$$
$$\hat{H}_{Zeeman} = -\alpha\,\beta H\hat{L}_{Co} \quad (2c)$$

where eqs 2a−2c account for the spin−orbit coupling of the six-coordinated high-spin Co^{II}, the axial distortion that splits the triplet orbital ground state T_1 into a singlet (A_2) and a doublet (E) level separated by a Δ energy gap, and the Zeeman interaction of the orbital part of the Co^{II} center, respectively. λ is the spin−orbit coupling constant, and α is

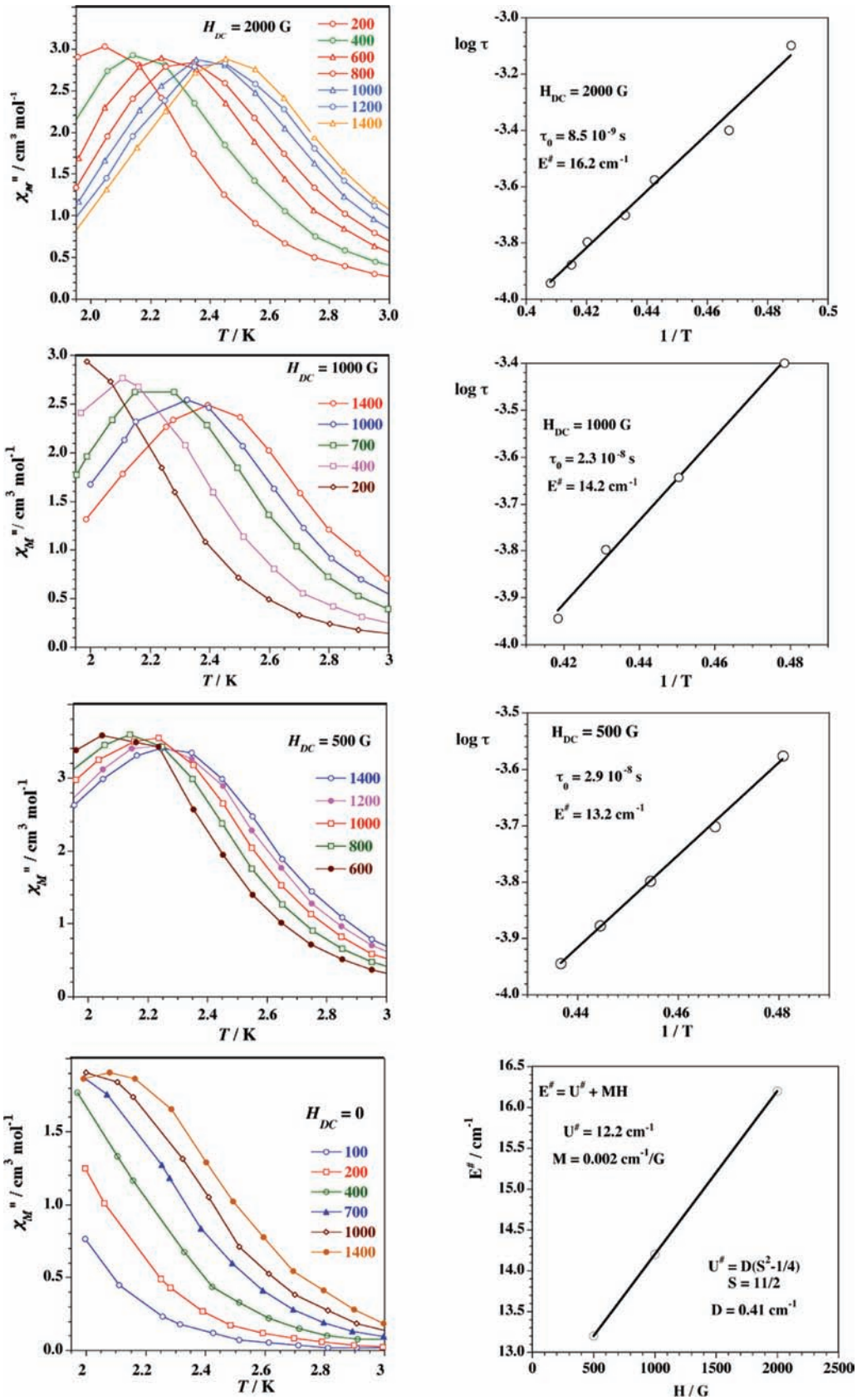

Figure 7. Left: Frequency and temperature dependence of the out-of-phase magnetic susceptibility under external applied dc magnetic fields of 2000, 1000, 500, and 0 G in a 1 G oscillating field and in the frequency range 100−1400 Hz for **4**. Right: Arrhenius plots as log τ vs $1/T$ obtained from ac measurements on a polycrystalline powder sample of **4** at different applied dc magnetic fields (top and middle) and field dependence of the energy barrier (bottom).

defined as $\alpha = Ak$, where A varies between $^3/_2$ (weak crystal field) and 1 (strong crystal field) and k is the orbital reduction factor due to covalency effects.[24a] The analysis of the magnetic susceptibility data of **3** through the Hamiltonians

of eqs 1 and 2 by using matrix diagonalization techniques leads to the best-fit parameters, which are listed in Table 2. The calculated curve (solid line in Figure 4) matches well the magnetic data from room temperature until the vicinity of the minimum of $\chi_M T$, with the mismatching between the experimental data and the calculated plot observed in the very low-temperature region being most likely due to the occurrence of weak intermolecular antiferromagnetic interactions and anisotropy effects. The values of λ, Δ, and k obtained by fitting are within the range of those reported for high-spin octahedral Co^{II} complexes.[24]

$\chi_M T$ at room temperature for **2** is equal to 8.20 $cm^3\ mol^{-1}$ K (Figure 5), a value that is consistent with the presence of a high-spin Fe^{II} ion ($S_{Fe} = 2$) and three Re^{IV} ions magnetically isolated. Upon cooling, this value increases to reach a rounded maximum of 9.36 $cm^3\ mol^{-1}$ K at 70.0 K and further decreases to 5.95 $cm^3\ mol^{-1}$ K at 1.9 K. This plot is as expected for a ferromagnetic coupling, with the decrease of $\chi_M T$ in the low-temperature domain being due to zfs effects. Although the ground-state term for a six-coordinated high-spin Fe^{II} (the case of **2**) is $^5T_{2g}$, the distortion of this six-coordinated Fe^{II} complex is large enough to fully quench the orbital contribution, allowing the successful application of the above Hamiltonian to the analysis of the magnetic data of **2** (see the solid line in Figure 5) with values of the best-fit parameters (see Table 2) that are physically reasonable.

Finally, the $\chi_M T$ vs T plot for **1** (Figure 6) continuously decreases upon cooling from 9.50 $cm^3\ mol^{-1}$ K at 300 K [$\chi_M T$ of ca. 9.20 $cm^3\ mol^{-1}$ K for one Mn^{II} ($S_{Mn} = {}^5/_2$) and three Re^{IV} ($S_{Re} = {}^3/_2$) ions magnetically isolated] to 1.75 $cm^3\ mol^{-1}$ K at 1.9 K. This decrease can be due to an antiferromagnetic interaction and/or zfs effects. The fact that the value of $\chi_M T$ at 1.9 K is well below that is calculated for a magnetically noninteracting four-spin set of three Re^{IV} and one Mn^{II} centers, $\chi_M T = 3 \times 1.0 + 4.375 = 7.38$ $cm^3\ mol^{-1}$ [$\chi_M T$ for a magnetically isolated Re^{IV} ion tends to 1.0 $cm^3\ mol^{-1}$ K in the low-temperature region, as indicated above] supports the occurrence of a significant intramolecular antiferromagnetic interaction in **1**. The analysis of its magnetic data through the Hamiltonian of eq 1 leads to the best-fit parameters that are listed in Table 2. The calculated plot matches well the magnetic data in the whole temperature range explored.

We finish this part with a brief discussion on the nature and magnitude of the magnetic coupling in this series of oxalato-bridged $Re^{IV}-M^{II}$ compounds. For the sake of simplicity, we will limit our discussion to a binuclear $Re^{IV}-M^{II}$ unit. The exchange-coupling parameter J_{ReM} is expressed by means of the individual interactions J_{ij} as in eq 3

$$J_{ReM} = (1/n_i n_j)\Sigma_{i,j} J_{ij} \qquad (3)$$

where n_i and n_j are the number of unpaired electrons on the Re^{IV} ($n_i = 3$) and M^{II} ions [$n_j = 1$ (Cu), 2 (Ni), 3 (Co), 4 (Fe), and 5 (Mn)], respectively.[26a,b] The strict orthogonality between the magnetic orbitals of the Re^{IV} (d^3 electronic configuration with three unpaired electrons in t_{2g}-type orbitals) and those of the Ni^{II}/Cu^{II} (two/one unpaired electrons in e_g-type orbitals) accounts for the ferromagnetic coupling observed in **4** and **5**. However, because the number of unpaired electrons on the t_{2g} orbitals increases when going from Co^{II} ($t_{2g}{}^5e_g{}^2$) to Mn^{II} ($t_{2g}{}^3e_g{}^2$), the possibilities of net overlap between interacting magnetic orbitals (and then the antiferromagnetic contributions) also increase. So, the antiferromagnetic terms become more and more important and the magnetic coupling, which is still ferromagnetic for **3** and **2**, becomes antiferromagnetic for **1**.[26c]

Slow Magnetic Relaxation in 4. (i) ac Study. Compound **4** exhibits frequency-dependent out-of-phase ac signals (χ_M'') at very low temperatures (left column, Figure 7). This feature is indicative of a system with slow relaxation of magnetization. No maxima of χ_M'' are observed above 1.9 K in the frequency range explored under a dc field $H_{dc} = 0$ G (bottom of the left column, Figure 7). However, maxima of χ_M'' appear at $T > 1.9$ K under applied dc magnetic fields of 500, 1000, and 2000 G, with their positions being shifted to higher temperatures with increasing field. The data obtained for each nonzero dc field were fit to the Arrhenius equation, with the corresponding values of τ_0 (preexponential factor) and E_a (energy barrier) being 8.5×10^{-9} s and 16.2 cm^{-1} ($H =$ 2000 G), 2.3×10^{-9} s and 14.2 cm^{-1} ($H_{dc} = 1000$ G), and 2.9×10^{-8} s and 13.2 cm^{-1} ($H_{dc} = 500$ G) (top and two middle plots of the right column in Figure 7). By extrapolation from these data, one can see that the value of τ_0 for $H_{dc} = 0$ G must be close to 3×10^{-8} s. A linear field dependence of the energy barrier with the applied dc field as $E_a = U^{\#} + MH$ also occurs with $M = 0.002$ $cm^{-1}\ G^{-1}$ (bottom plot of the right column, Figure 7). This dependence allows the evaluation of $U^{\#} = 12.2$ cm^{-1} for $H_{dc} = 0$. Given that in the present case $U^{\#} = |D_{11/2}|$ ($S^2 - {}^1/_4$) with $S = {}^{11}/_2$, a value of 0.41 cm^{-1} is derived for $|D_{11/2}|$. This value is in reasonable agreement with those obtained for this parameter through the above fit of the $\chi_M T$ data.

The χ_M'' vs χ_M' plots (Cole−Cole plots)[27] in the frequency range 200−400 GHz at different temperatures and dc field values for **4** give semicircles (Figure 8). Least-squares fit of the experimental data through the Cole−Cole expression (eq 4)[27,28]

$$\chi = \chi_S + \frac{\chi_T - \chi_S}{1 + (i\omega\tau)^{1-\alpha}} \qquad (4)$$

where χ_S and χ_T are the adiabatic and isothermal susceptibilities, gave small values of α under dc fields varying in the

(24) (a) Lloret, F.; Julve, M.; Cano, J.; Ruiz-García, R.; Pardo, E. *Inorg. Chim. Acta* **2008**, *361*, 3432. (b) Mishra, V.; Lloret, F.; Mukherjee, R. *Inorg. Chim. Acta* **2006**, *359*, 4053. (c) Herrera, J. M.; Bleuzen, A.; Dromzée, Y.; Julve, M.; Lloret, F.; Verdaguer, M. *Inorg. Chem.* **2003**, *42*, 7052. (d) Colacio, E.; Lloret, F.; Ben-Maimoun, I.; Kivekas, R.; Sillanpaa, R.; Suárez-Varela, J. *Inorg. Chem.* **2003**, *42*, 2720.
(25) Figgis, B. N.; Gerloch, M.; Lewis, J.; Mabbs, F. E.; Webb, G. A. *J. Chem. Soc. A* **1968**, 2086.
(26) (a) Girerd, J. J.; Charlot, M. F.; Kahn, O. *Mol. Phys.* **1977**, *34*, 1063. (b) Charlot, M. F.; Girerd, J. J.; Kahn, O. *Phys. Status Solidi B* **1978**, *86*, 497. (c) Kahn, O. *Molecular Magnetism*; VCH: New York, 1993; pp 190−198.
(27) Cole, K. S.; Cole, R. H. *J. Chem. Phys.* **1941**, *9*, 341.
(28) (a) Boettcher, C. J. F. *Theory of Electric Polarization*; Elsevier: Amsterdam, The Netherlands, 1952. (b) Aubin, S. M.; Sun, Z.; Pardi, L.; Krzystek, J.; Folting, K.; Brunel, L. J.; Rheingold, A. L.; Christou, G.; Hendrickson, D. N. *Inorg. Chem.* **1999**, *38*, 5329.

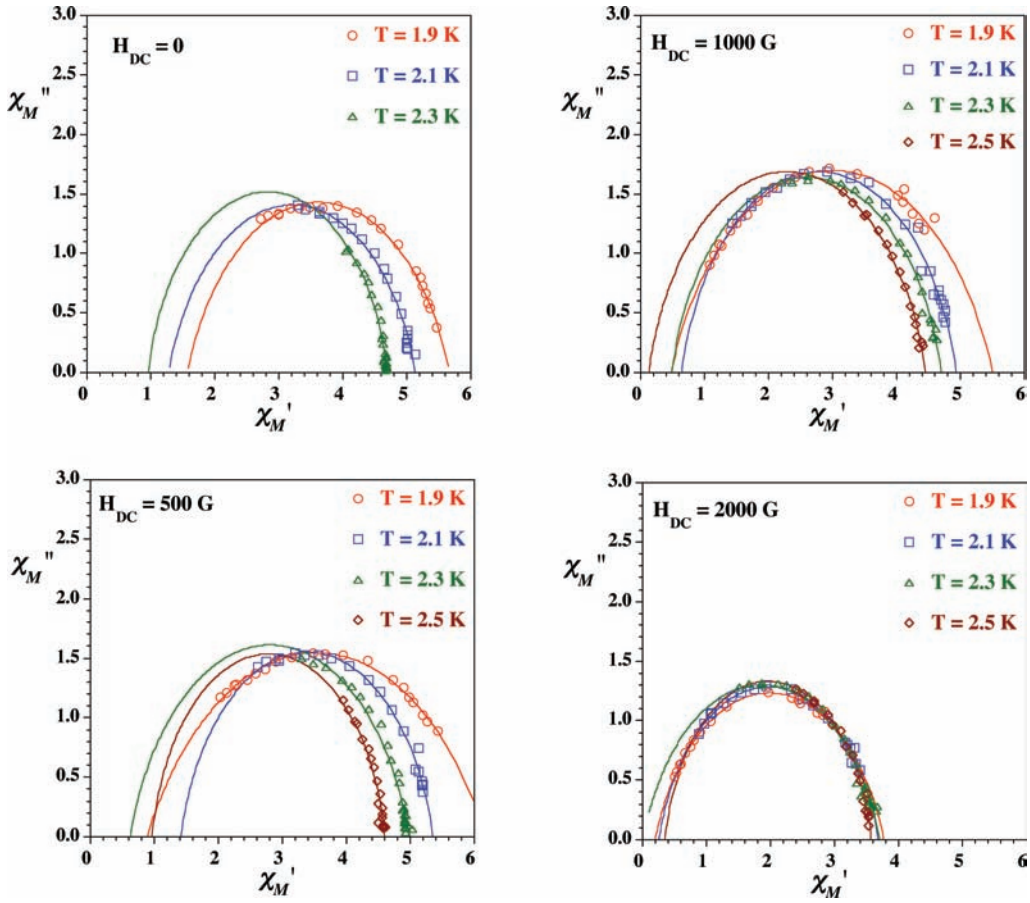

Figure 8. Cole−Cole plots (χ_M'' vs χ_M') for **4** obtained from ac measurements at different temperatures and applied dc magnetic fields of 0, 500, 1000, and 2000 G. The solid lines are the best-fit curves (see the text).

range of 0−2000 G (see Table S2 in the Supporting Information). One can see therein that for each applied dc field the values of α increase as T decreases in the temperature range 1.9−2.5 K, indicating that intermolecular magnetic interactions occur in the very low-temperature range. Finally, keeping in mind that $\alpha = 0$ for an ideal Debye model with a single relaxation time, the small values of α allow one to discard a spin-glass behavior for **4**.[29]

(ii) HFEPR Investigation. In an attempt to substantiate both the sign and magnitude of the zfs in **4**, which are difficult to determine from magnetic susceptibility measurements on powder samples, and given the relevance of this parameter to the slow relaxation of magnetization that occurs in the SMMs, we carried out a HFEPR study to evaluate this parameter more accurately. Complex **4** indeed produced very rich spectra at low temperatures (4.2 K), which are, however, very different from those typically observed in SMMs.[30,31] In particular, we could find no usual progression

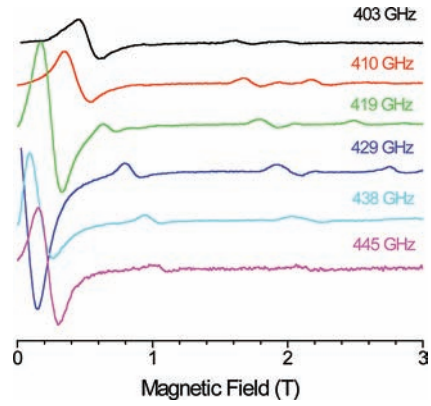

Figure 9. EPR resonances in polycrystalline **4** observed in the vicinity of the zf resonance at ~430 GHz and 4.2 K. The frequency is indicated next to each trace.

of resonances in high magnetic fields representing the allowed ($\Delta M_S = \pm 1$) transitions within the $S = {}^{11}/_{2}$ ground state of the complex. Instead, a number of resonances are present at high frequencies but only low fields. By extrapolating these to zero field (zf), we could find four zf resonances, of which the most prominent one appeared at 430 ± 5 GHz (Figure 9) and others at about 250, 340, and 660 GHz. The presence of further zf resonances was suggested by the appearance of additional signals at applied fields (Figure S6 in the Supporting Information). All of the observed resonances quickly broaden and disappear upon moving the field to values higher than 2−5 T. We interpret

(29) (a) Chowdhury, D. *Spin Glasses and Other Frustrated Systems*; Princeton University Press: Princeton, NJ, 1986. (b) Moorjani, K.; Coey, J. M. *Magnetic Glasses*; Elsevier: New York, 1984. (c) Binder, K.; Young, A. P. *Rev. Mod. Phys.* **1986**, *58*, 801. (d) Mydosh, J. A. *Spin Glasses: An Experimental Introduction*; Taylor & Francis: London, 1993. (e) Girtu, M. A.; Wynn, C. M.; Fujita, W.; Awaga, K.; Epstein, A. *J. Phys. Rev. B* **1998**, *57*, R11058.
(30) Caneschi, A.; Gatteschi, D.; Sessoli, R.; Barra, A.-L.; Brunel, L. C.; Guillot, M. *J. Am. Chem. Soc.* **1991**, *113*, 5873.
(31) Barra, A. L.; DeBrunner, P.; Gatteschi, D.; Schulz, Ch. E.; Sessoli, R. *Europhys. Lett.* **1996**, *35*, 133.

them as $\Delta M_S \geq 1$ transitions appearing between the low-lying ($M_S = \pm{}^{11}/_2$ and $\pm{}^{9}/_2$) and higher ($M_S = \pm{}^{7}/_2$, $\pm{}^{5}/_2$, etc.) Kramers doublets. To derive the parameters of interest from our data, we plotted the observed resonances as a two-dimensional field-frequency map along the principles of tunable-frequency EPR[32] and compared them to simulations. We found out that there is only one possible set of parameters that adequately simulates the observed dependencies (Figure S6 in the Supporting Information): $|D| = 0.8(1)$ cm^{-1}, $E \sim 0$, and $g = 2.0$. The agreement is not perfect, suggesting the presence of a rhombic zfs parameter E, and possibly higher-ranking zfs parameters, which are difficult to extract in zf. Establishing the sign of D is somewhat more problematic than establishing its magnitude. To solve this problem, we drafted the energy diagram of zf M_S states for $S = {}^{11}/_2$ using the spin Hamiltonian parameter set obtained above (Figure S7 in the Supporting Information). The observed sequence of zf resonances (250, 340, 430, and 660 GHz) fits the diagram drafted for negative D (where they would correspond to transitions ($|M_S| = {}^{11}/_2 \rightarrow {}^{9}/_2$, ${}^{9}/_2 \rightarrow {}^{5}/_2$, ${}^{11}/_2 \rightarrow {}^{7}/_2$, and ${}^{11}/_2 \rightarrow {}^{3}/_2$, respectively) much better than that for positive D (where they would correspond to transitions $|M_S| = {}^{3}/_2 \rightarrow {}^{7}/_2$, ${}^{5}/_2 \rightarrow {}^{9}/_2$, ${}^{3}/_2 \rightarrow {}^{9}/_2$, and ${}^{3}/_2 \rightarrow {}^{11}/_2$, respectively) under a logical assumption that at low temperature it is the ground state $|M_S|$ (${}^{11}/_2$ in the first case and ${}^{1}/_2$ in the latter case) that is most populated. This gives a strong argument for the negative D case.

The absence of resonances at high fields remains puzzling. We can only speculate about a particularly strong field dependence of relaxation rates in the system of interest, which may broaden the expected resonances beyond recognition. Whether this is characteristic for clusters containing a heavy element such as Re remains to be further investigated by subjecting a larger number of similar systems to EPR investigations.

(iii) Micro-SQUID Study. To further explore the SMM behavior of **4** at very low temperatures, single-crystal magnetization measurements were performed with an array of micro-SQUID studies at temperatures close to 40 mK. The measurements were performed with the magnetic field parallel to the easy axis of the crystal. Hysteresis loops for **4** at different temperatures and sweep rates are shown in Figure 10. These curves show that an extremely fast tunneling occurs at zero applied dc field. However, when $H > 0$ G, the tunneling is switched off and temperature- and sweep-rate-dependent coercivity occurs, a behavior that was previously observed in cyano-bridged heterometallic species.[33] The data obtained at a sweep rate of 0.14 T s^{-1} show a hysteresis loop that includes two steps: a broad one at about 0.3 T and the other very close to zero (Figure 10, middle). The presence of a hysteresis loop indicates that below 1.0 K the magnetization is blocked. As the temperature decreases, the number of units that undergo relaxation by thermal activation diminishes and those that undergo relaxation by tunneling increases. The result is a narrowing of the hysteresis loop with steeper steps. The tunnel probability decreases when the sweep rate is increased,[34] with the number of molecules tunneling at zf being less important and the hysteresis loop being larger, as shown in Figure 10 (bottom).

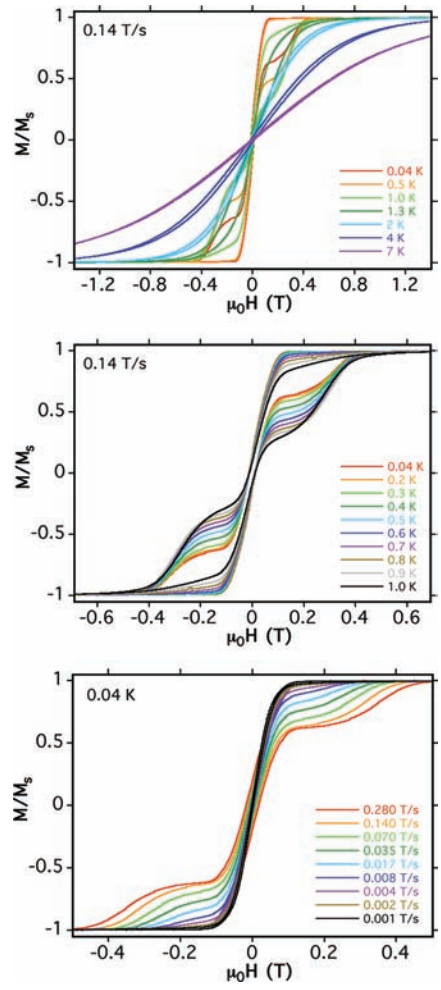

Figure 10. Magnetization (M) (plotted as a fraction of the maximum value M_S) vs applied field ($\mu_0 H$) recorded on a single crystal of **4**. The resulting loops are shown at different temperatures (top, middle) and different field sweep rates (bottom).

The question at hand now is why does only compound **4** exhibit SMM behavior and not compounds **2** and **3**, where a high-spin ground state and important local anisotropies coexist. Comparing **4** with its congeners (**2**, **3**, and **5**), one can see that all of them show similar crystallographic features. However, there is a significant structural difference between them that would account for this situation. In this series, the surroundings of the M atom are practically of D_3 symmetry. In that respect, following previous works dealing with the study of the SMM phenomenon in tetranuclear Fe^{III} complexes with $S = 5$ as the ground-state spin,[35,36] two types of distortion for an octahedron, which are defined by the θ (trigonal compression/elongation) and ϕ (trigonal rotation) angles, have been identified as relevant parameters to observe

(32) Krzystek, J.; Zvyagin, S. A.; Ozarowski, A.; Trofimenko, S.; Telser, J. *J. Magn. Reson.* **2006**, *178*, 174.
(33) (a) Rebilly, J. N.; Catala, L.; Guillot, R.; Wernsdorfer, W.; Mallah, T. *Inorg. Chem.* **2005**, *44*, 8194. (b) Rebilly, J. N.; Catala, L.; Rivière, E.; Guillot, R.; Wernsdorfer, W.; Mallah, T. *Chem. Commun.* **2006**, 735.
(34) Wernsdorfer, W.; Sessoli, R. *Science* **1999**, *284*, 133.
(35) Gatteschi, D.; Sorace, L. *J. Solid State Chem.* **2001**, *159*, 253.

SMM behavior. If we focus on trigonal rotation and the twist angle ϕ, we see that compound **4** shows the largest distortion because the value of ϕ departs by more than 10° from that of the regular octahedron ($\phi = 60°$) while in **2**, **3**, and **5**, the corresponding values are very close to the ideal one (see above in the structural description). Furthermore, angular overlap model calculations have shown that a higher trigonal rotation favors a negative value of the anisotropy (D), with this last fact being necessary to observe the SMM phenomenon.[35]

Conclusions

In summary, a novel series of heterotetranuclear $Re^{IV}_3M^{II}$ compounds have been prepared using the $[ReCl_4(ox)]^{2-}$ complex as a ligand toward fully solvated M^{II} ions [M = Mn (**1**), Fe (**2**), Co (**3**), Ni (**4**), and Cu (**5**)] where the tetranuclear $[\{ReCl_4(ox)\}_3M]^{4-}$ anions are well separated from each other by bulky NBu_4^+ cations. Once more the oxalato ligand appears as a good bridging ligand that is able to mediate significant ferromagnetic (**2**−**5**) and antiferromagnetic (**1**) exchange interactions between the paramagnetic metal ions that it connects. The Ni^{II} derivative (**4**) is the first example of a Re^{IV}-containing compound that shows SMM behavior, being described either as a SMM with a fast tunnel transition at $H = 0$ G or as a compound whose SMM behavior is only "switched-on" by the application of an external magnetic field. Anyway, this work shows that the combination of Re^{IV} ($S_{Re} = {}^3/_2$ with a large anisotropy) and other anisotropic metal ions in the same molecular species will provide new families of SMMs with exciting magnetic properties.

Acknowledgment. Financial support from the Ministerio Español de Educación y Ciencia (Project CTQ2007-61690), the Italian Ministero dell'Istruzione, dell'Università e della Ricerca, and the Consolider Ingenio in Molecular Nanoscience CSD2007-00010 is gratefully acknowledged. HFEPR studies were supported by the NHMFL, which is funded by the NSF through Cooperative Agreement DMR 0654118, the State of Florida, and the DOE. J.K. acknowledges Universitat de València for a visiting Professor fellowship.

Supporting Information Available: X-ray crystallographic files (CIF) for compounds **2**−**5**, structural drawings of the heterotetranuclear units of **3**−**5** (Figures S1−S3) and packing diagrams for **2**−**5** (Figures S4 and S5), selected bond lengths and angles for **2**−**5** (Tables S1 and S2), a field versus frequency map of EPR resonances for **4** at 4.2 K (Figure S6), and the energy diagram of the zf M_S states in the cases of negative and positive D for **4** (Figure S7). This material is available free of charge via the Internet at http://pubs.acs.org. The crystallographic files are also available upon application to the Cambridge Crystallographic Data Centre, 12 Union Road, Cambridge CB2 1EZ, U.K. [fax (+44) 1223-336-033; e-mail deposit@ccdc.cam.ac.uk]: CCDC 703486 (**2**), 703487 (**3**), 609801 (**4**), and 703488 (**5**).

IC8021497

(36) (a) Cornia, A.; Fabretti, A. C.; Garrisi, P.; Mortalò, C.; Bonacchi, D.; Gatteschi, D.; Sessoli, R.; Sorace, L.; Wernsdorfer, W.; Barra, A. L. *Angew. Chem., Int. Ed.* **2004**, *43*, 1136. (b) Accorsi, S.; Barra, A. L.; Caneschi, A.; Chastanet, G.; Cornia, A.; Fabretti, A. C.; Gatteschi, D.; Mortalò, C.; Olivieri, E.; Parenti, F.; Rosa, P.; Sessoli, R.; Sorace, L.; Wernsdorfer, W.; Zobbi, L. *J. Am. Chem. Soc.* **2006**, *128*, 4742.